ACS APPLIED MATERIALS & INTERFACES

Research Article

Cite This: ACS Appl. Mater. Interfaces 2019, 11, 44501−44512

www.acsami.org

Regulation of Molecular Packing and Blend Morphology by Finely Tuning Molecular Conformation for High-Performance Nonfullerene Polymer Solar Cells

Xunchang Wang,[†,‡] Jianhua Han,[†] Huanxiang Jiang,[†,‡] Zhilin Liu,[†] Yonghai Li,[†] Chunming Yang,[§] Donghong Yu,[∥] Xichang Bao,*[†] and Renqiang Yang*[,†]

[†]CAS Key Laboratory of Bio-Based Materials, Qingdao Institute of Bioenergy and Bioprocess Technology, Chinese Academy of Sciences, Qingdao 266101, Shandong, China

[‡]Center of Materials Science and Optoelectronics Engineering, University of Chinese Academy of Sciences, Beijing 100049, Beijing, China

[§]Shanghai Synchrotron Radiation Facility, Shanghai Institute of Applied Physics, Chinese Academy of Sciences, Shanghai 201204, Jiangsu, China

[∥]Department of Chemistry and Bioscience, Aalborg University, Aalborg East DK-9220, North Jutland Region, Denmark

Supporting Information

ABSTRACT: The asymmetric thienobenzodithiophene (TBD) structure is first systematically compared with the benzo[1,2-*b*:4,5-*b*′]dithiophene (BDT) and dithieno[2,3-*d*:2′,3′-*d*′]benzo[1,2-*b*:4,5-*b*′]dithiophene (DTBDT) units in donor−acceptor (D−A) copolymers and applied as the central core in small molecule acceptors (SMAs). Specific polymers including PBDT-BZ, PTBD-BZ, and PDTBDT-BZ with different macromolecular conformations are synthesized and then matched with four elaborately designed acceptor−donor−acceptor (A−D−A) SMAs with structures comparable to their donor counterparts. The resulting polymer solar cell performance trends are dramatically different from each other and highly material-dependent, and the active layer morphology is largely governed by polymer conformation. Because of its more linear backbone, the PTBD-BZ film has higher crystallinity and more ordered and denser π−π stacking than those of the PBDT-BZ and PDTBDT-BZ films. Thus, PTBD-BZ shows excellent compatibility with and strong independence on the SMAs with varied structures, and PTBD-BZ-based cells deliver high power conversion efficiency (PCE) of 10−12.5%, whereas low PCE is obtained by cells based on PDTBDT-BZ because of its zigzag conformation. Overall, this study reveals control of molecular conformation as a useful approach to modulate the photovoltaic properties of conjugated polymers.

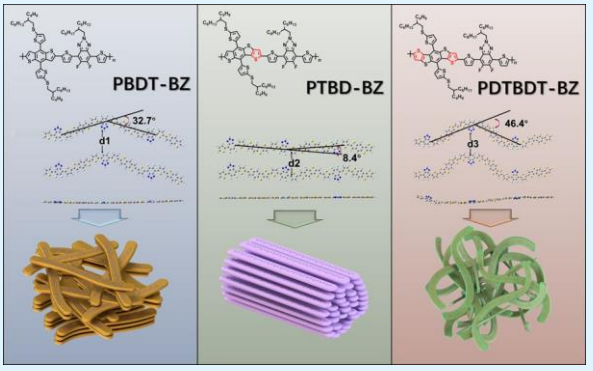

KEYWORDS: *nonfullerene solar cell, asymmetrical backbone, molecular conformation, morphology, power conversion efficiency*

INTRODUCTION

Nonfullerene polymer solar cells (PSCs) based on polymer donor/small molecular acceptor (SMA) bulk heterojunctions (BHJs) have developed rapidly in the past few years.[1−8] Benefitting from extensive research, power conversion efficiencies (PCEs) exceeding 14−16 and 17% have been realized in single junction cells and in tandem solar cells, respectively.[9−19] In high-performance device systems, a polymer donor and a SMA should have complementary absorption to realize a high short-circuit current (J_{sc}), a fine-tuned energy level to obtain a high open-circuit voltage (V_{oc}), and compatible morphology to achieve an excellent fill factor (FF).[20−23] In fact, engineering such microcosmic morphology of BHJ blends remains extremely challenging, as the appropriate selection of the polymer donor and the SMA involves the art of balancing several considerations, such as crystallinity, phase separation, and pure domain size.[24−28]

As we know, molecular conformation is regarded as an important factor affecting BHJ film morphology, although morphology can be further optimized by postprocessing.[29−32] To date, many strategies involving modifying molecular conformation have been applied to polymer donors to achieve improved film morphology.[33−43] For instance, Hou and coworkers tailored the backbone of the polymer PBDTTT-S-T from a zigzag to a linear structure by replacing the benzo[1,2-*b*:4,5-*b*′]dithiophene (BDT) unit with a dithieno-

Received: August 23, 2019
Accepted: November 1, 2019
Published: November 1, 2019

DOI: 10.1021/acsami.9b14981
ACS Appl. Mater. Interfaces 2019, 11, 44501−44512

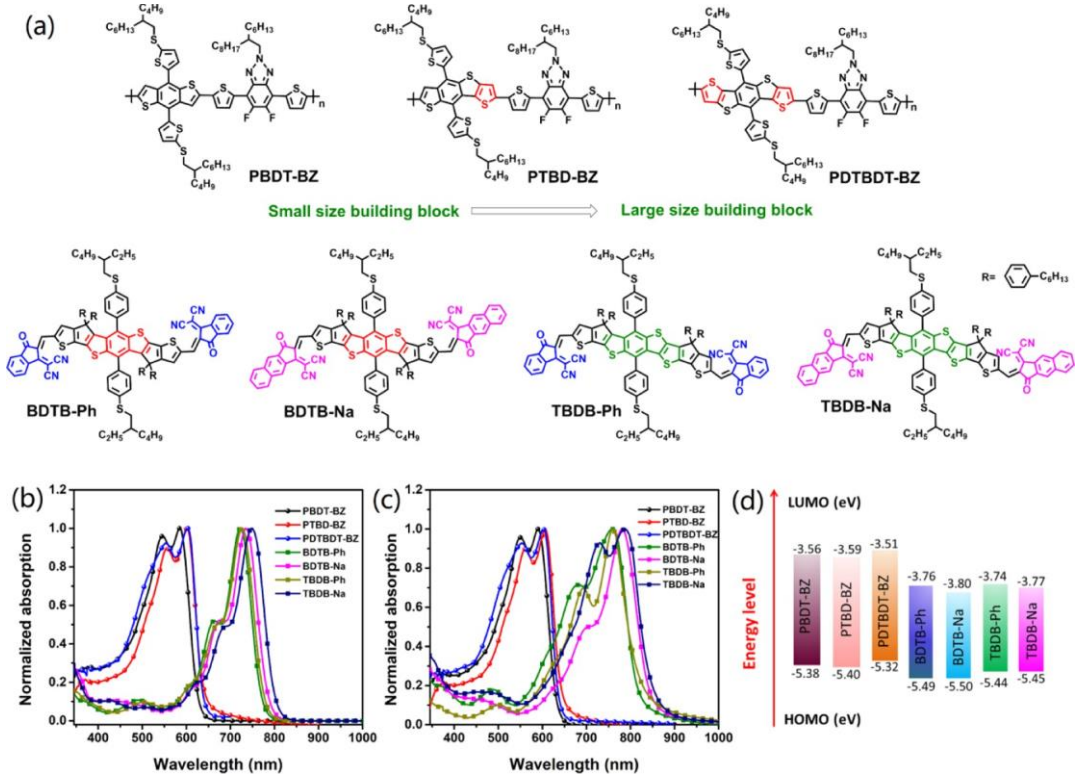

Figure 1. (a) Chemical structures of the donor polymers and acceptor molecules used in this study. Normalized ultraviolet−visible absorption spectra of the donor polymers in (b) dilute CB solution and (c) neat films. (d) Energy-level diagram of thin films obtained from CV measurements.

[2,3-*d*:2′,3′-*d*′]benzo[1,2-*b*:4,5-*b*′]dithiophene (DTBDT) unit, and the resultant polymer PDT-S-T exhibited stronger intermolecular π−π stacking and more ordered lamellar packing properties with improved photovoltaic (PV) performance.[33] Very recently, a few research groups reported encouraging results by employing rigid or large conjugated segments to prohibit excessive interchain aggregation. For example, Yan et al. reported the DFBT-based polymer PTFB-O with a less symmetric monomer unit inserted in the backbone, which showed less crystalline properties but performed better in nonfullerene organic solar cells (OSCs).[38] Moreover, a π bridge is an effective method commonly used to modulate backbone planarity and control morphology. In our previous work, compared with the random polymer PBTzT-4, the regioregular polymer PBTzT-4R with a directional thiazole moiety exhibited a more planar backbone with higher crystallinity and denser π−π stacking, leading to superior PV performance.[41] All the above results indicate that the morphology of a conjugated polymer is closely correlated with its molecular backbone conformation.

In addition to polymer donor backbone modification, the conformation of acceptor−donor−acceptor (A−D−A)-type SMAs may also play a critical role in BHJ morphology. The central "D" core and the terminal "A" group, as well as the side chain, can simultaneously influence the molecular packing and miscibility of the BHJ film.[17,44−58] To date, most of the reported SMAs with an A−D−A architecture have featured benzothiadiazole (BT),[18,19,59] indacenodithieno[3,2-*b*]-thiophene (IDTT),[60,61] BDT,[62] or thieno[3,2-*b*]thiophene[48,63] as the D core and 2-(3-oxo-2,3-dihydro-1*H*-inden-1-ylidene)-malononitrile (INCN),[60] thiophene-fused indanone (CPTCN),[53,64] and naphthyl-fused indanone (NINCN)[51,52] as the terminal A groups. Considering the large number of central D cores and terminal A groups, delicate tailoring and proper combination of such D and A structures through fine molecular design are of great importance.

Unfortunately, despite the tremendous efforts toward designing new polymer donors and SMAs, fine control of molecular conformation and the correlation among molecular conformation, crystallinity, orientation, and PV performance have seldom been examined simultaneously. Therefore, the design of a rational structure to facilitate the control of PSC morphology and improve PSC performance would be both interesting and challenging.

In this work, different backbone materials, including different polymer donors (PBDT-BZ, PTBD-BZ, and PDTBDT-BZ) and SMAs (BDTB-Ph, BDTB-Na, TBDB-Ph, and TBDB-Na), were rationally designed and synthesized to systematically study the compatibility of polymer/acceptor models. In particular, the asymmetric thienobenzodithiophene (TBD) structure was first compared with the BDT and DTBDT units in D−A copolymers and first applied as the central core in SMAs. PDTBDT-BZ with a zigzag backbone (46.4°) displays amorphous stacking, which is not compatible with all the four SMAs. The polymer PBDT-BZ with an angle of 32.7° in the backbone presented moderate crystallinity and yielded quite low-efficiency OSCs when combined with two BDT-based SMAs, but it matched well with two TBD-based SMAs. The main reason for the varied performance may be that PBDT-BZ destroys the original packing properties and changes the mixed face-on/edge-on textures of BHJ films. In contrast, the polymer PTBD-BZ with an asymmetric TBD segment shows an extremely linear backbone conformation with strong and dense intermolecular stacking. This polymer can not only perform well in conjunction with SMAs based on the BDT core but also provides highly efficient devices with

DOI: 10.1021/acsami.9b14981
ACS Appl. Mater. Interfaces 2019, 11, 44501−44512

Table 1. Summary of the Optical Properties of the Polymers and SMAs

materials	ε^{a} [M^{-1} cm^{-1}]	λ^{film} [nm]	λ [nm]	$E^{opt}{}^{b}$ [eV]	HOMO[c] [eV]	LUMO[c] [eV]
PBDT-BZ	7.6×10^4	590	646	1.92	−5.38	−3.56
PTBD-BZ	8.3×10^4	601	652	1.90	−5.40	−3.59
PDTBDT-BZ	6.8×10^4	598	648	1.91	−5.32	−3.51
BDTB-Ph	1.9×10^5	759	835	1.48	−5.49	−3.76
BDTB-Na	2.3×10^5	781	871	1.42	−5.50	−3.80
TBDB-Ph	1.6×10^5	760	848	1.46	−5.44	−3.74
TBDB-Na	2.1×10^5	786	877	1.41	−5.45	−3.77

[a]In CB solution. [b]Calculated from the empirical formula $E_g^{opt} = 1240/\lambda_{onset}$. [c]Obtained from the CV method.

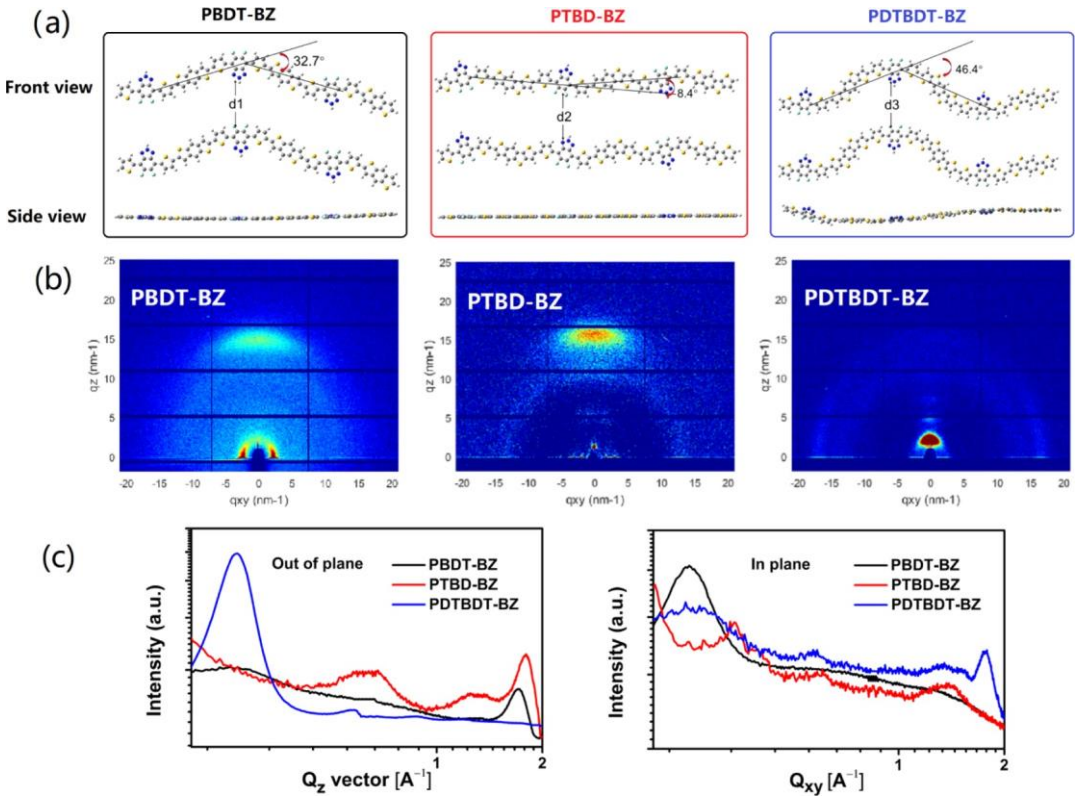

Figure 2. (a) Backbone conformations of the three polymers PBDT-BZ, PTBD-BZ, and PDTBDT-BZ. These conformation were obtained by DFT at the B3LYP/6-31G(d,p) level; (b) GIWAXS diffractograms of PBDT-BZ, PTBD-BZ, and PDTBDT-BZ; and (c) 1D diffraction profiles of the three donor polymers in the OOP and IP orientations.

PCEs increased to 11.0 and 12.47% when combined with SMAs based on the TBD core. The high performance is attributed to the improved crystallinity and face-on orientation as well as the balanced pure domain size and miscibility, which can be verified by grazing-incidence wide-angle X-ray scattering (GIWAXS) analysis and the Flory−Huggins interaction parameter (χ). Furthermore, the results reveal the relationship between polymer/SMA molecular conformation and morphology, as well as compatibility, which shows that molecular conformation and crystallinity are important factors for designing new organic PV materials.

RESULTS AND DISCUSSION

The chemical structures of the three similar donor polymers and four SMAs are illustrated in Figure 1a. The detailed synthetic procedures for the small molecules are provided in the Supporting Information (Scheme S1). 4,7-Bis(5-bromothiophen-2-yl)-5,6-difluoro-2-(2-hexyldodecyl)-2*H*-benzo[*d*][1,2,3]triazole, which is one of the state-of-the-art electron acceptors utilized in conjugated polymers, was the only acceptor group used in this work.[65,66] All the D−A polymers and SMAs featured alkylthio groups on the side chain to further control the aggregation and energy level.[67−70] The three donor polymers have different-sized donor building blocks, BDT, TBD, and DTBDT, which possess three to five fused rings. The number average molecular weights (M_n) of PBDT-BZ, PTBD-BZ, and PDTBDT-BZ are 34.2, 39.2, and 35.3 kDa, respectively. The four acceptors with the same side chains can be divided into two groups: two symmetric acceptors, BDTB-Ph and BDTB-Na, based on the BDT core and two asymmetric acceptors, TBD-Ph and TBD-Na, based on the TBD core, which can successively expand the scope of potential skeletons.

Normalized ultraviolet−visible absorption spectra of the polymers and small molecules in both dilute chlorobenzene (CB) solutions and thin films at ambient temperature are shown in Figure 1b,c, and the related properties are summarized in Table 1. All the polymers display broad

DOI: 10.1021/acsami.9b14981
ACS Appl. Mater. Interfaces 2019, 11, 44501−44512

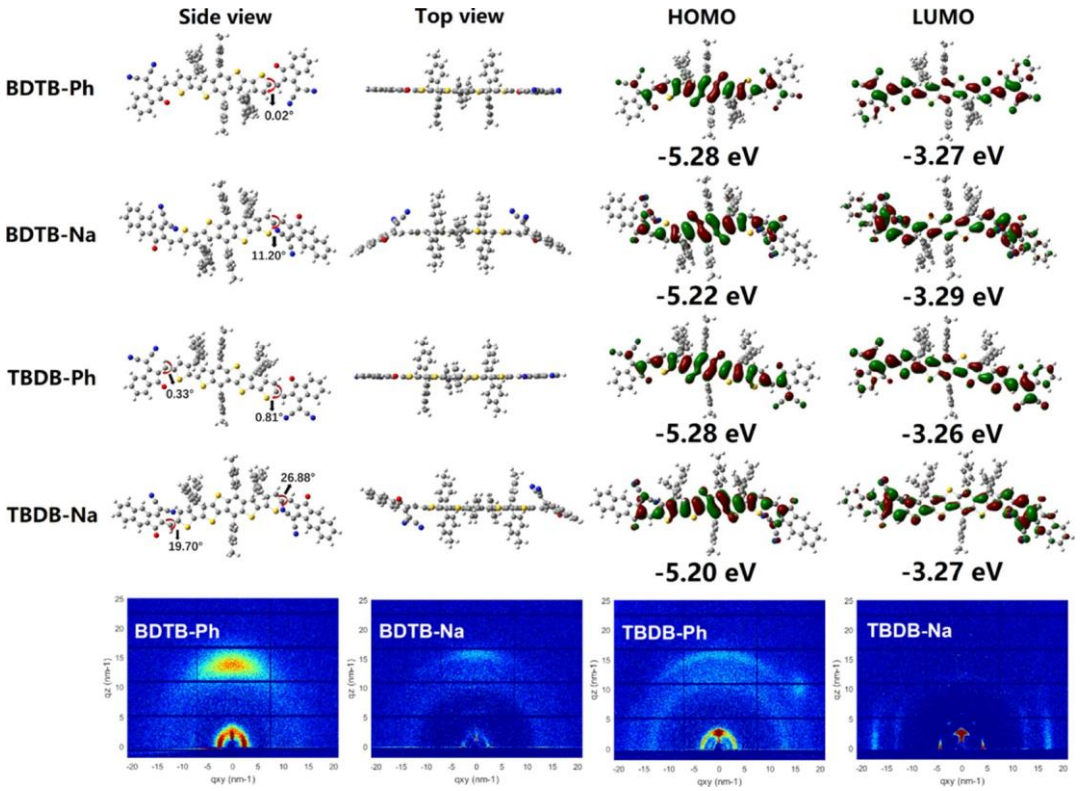

Figure 3. Optimized geometries (top) and GIWAXS diffractograms (down) of the four SMAs.

absorption in the range from 450 to 630 nm and show almost identical absorption onset at ca. 650 nm in both solution and solid films, corresponding to an optical band gap (E_g^{opt}) of ca. 1.90 eV. In CB solution, the molar absorption coefficients are $7.6 \times 10^4\ M^{-1}\ cm^{-1}$ for PBDT-BZ, $8.3 \times 10^4\ M^{-1}\ cm^{-1}$ for PTBD-BZ, and $6.8 \times 10^4\ M^{-1}\ cm^{-1}$ for PDTBDT-BZ. Notably, compared with the PDTBDT-BZ film, the PTBD-BZ film exhibits a slightly redshifted maximum absorption wavelength even though the former has an extended conjugated building block, which may be ascribed to the stronger π−π stacking of PTBD-BZ than PDTBDT-BZ. The four small molecules BDTB-Ph, TBDB-Ph, BDTB-Na, and TBDB-Na exhibit different absorption profiles and bandwidths in both solution and thin films, but the maximum absorption peaks of their films redshifted from 759 to 786 nm with increasing conjugation length (Figure 1c). It can be concluded that the absorption of both polymers and SMAs is indeed associated with the molecular backbone conformation. Thin-film cyclic voltammograms (CVs) of the polymers and small molecules were measured, as shown in Figure S1, and the energy levels were estimated according to the equation $E_{(HOMO/LUMO)} = -(E_{ox/red} + 4.36)$ (eV) (Figure 1d and Table 1). It can be observed that the HOMO energy levels of PTBD-BZ and PBDT-BZ are similar and slightly lower than that of PDTBDT-BZ. A possible reason for this phenomenon is that when the BDT unit is added at the [*d*,*d*′] position by fusing two thiophene rings, the obtained DTBDT unit may have a stronger electron-donating effect than that of the BDT and TBD units, therefore leading to a higher oxidation potential.[65] As a lower HOMO of the polymer donor is beneficial for achieving a higher V_{oc}, the replacement of BDT with TBD in the backbone may have no negative influence on the V_{oc} of PSCs compared with that of polymers in which BDT was replaced by DTBDT units.[33] The LUMO levels of the four small molecules were estimated from the onset reduction potentials to be −3.76, −3.80, −3.74, and −3.77 eV for BDTB-Ph, BDTB-Na, TBDB-Ph, and TBDB-Na, respectively.

Figure 2a shows the optimized backbone geometries of the polymers PBDT-BZ, PTBD-BZ, and PDTBDT-BZ obtained by theoretical calculation using density functional theory (DFT) at the B3LYP/6-31G* level. Because of the distinct conformations of the electron-rich units (BDT, TBD and DTBDT) and BZ building blocks, the polymers show entirely different backbone angles, which consist of the extended two adjacent D−A repeating units. PDTBDT-BZ has a zigzag backbone and shows angles of 46.4°, which may have a negative impact on polymer crystallinity. In contrast, PTBD-BZ shows an angle of 8.4° because of the asymmetric conformation of the TBD and BZ building blocks. Therefore, it can facilitate interdigitation of the polymer backbone to achieve ordered packing in the solid film.[71−73] The angle in the PBDT-BZ backbone is calculated to be 32.7°. To further support the theoretical calculation and study the relationship between the chemical backbone structures and film microstructures of the three polymers, we characterized these three pure polymer films by GIWAXS analysis and compared their crystallinity and packing orientation properties. As we know, high crystallinity of materials signifies more ordered packing, larger crystallite size, and less amorphous parts in thin films, which can be evaluated in GIWAXS patterns (sharp and well-defined diffraction spots). Clearly, both PBDT-BZ and PTBD-BZ exhibit distinct π−π stacking peaks in only the out-of-plane (OOP) direction, indicating a preferential face-on orientation of the two polymer films. Furthermore, the diffraction intensity of PTBD-BZ is stronger than that of PBDT-BZ, which could result from a more coplanar conformation. In contrast, a weak

DOI: 10.1021/acsami.9b14981
ACS Appl. Mater. Interfaces 2019, 11, 44501−44512

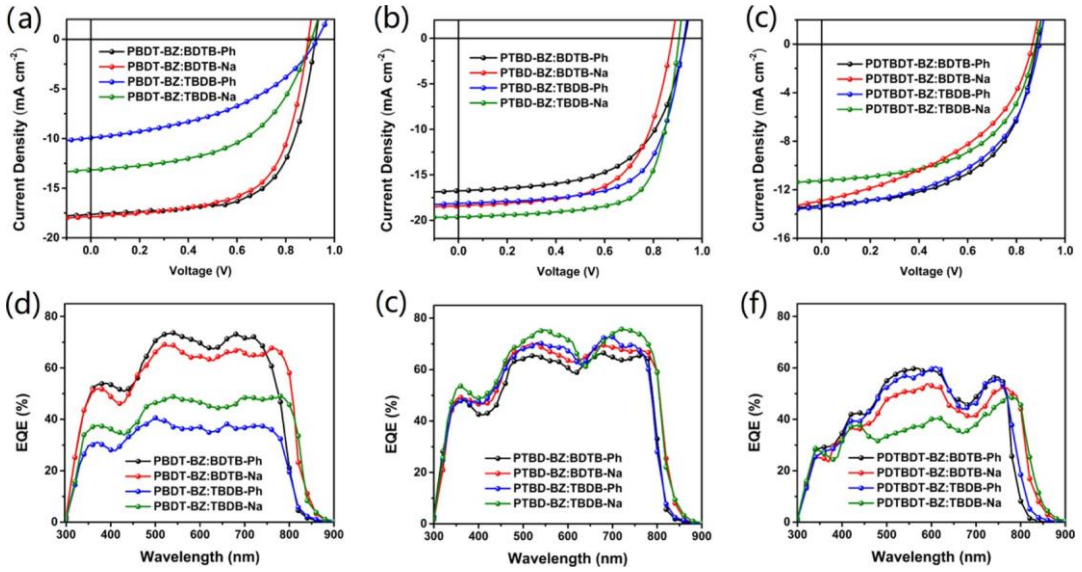

Figure 4. $J-V$ curves for the optimized devices under AM 1.5G illumination, 100 mW cm^{-2}: (a) PBDT-BZ-based devices; (b) PTBD-BZ-based devices; and (c) PDTBDT-BZ-based devices. EQE curves of the corresponding PSCs: (d) PBDT-BZ-based devices; (e) PTBD-BZ-based devices; and (f) PDTBDT-BZ-based devices.

Table 2. Device Parameters of the PSCs under AM 1.5G Illumination, 100 mW cm^{-2}

polymers	acceptors	V_{oc} (V^{avg})[a] [V]	J_{sc} (J^{avg})[a] [mA cm^{-2}]	J^{EQE}[b] [mA cm^{-2}]	FF (FF$_{avg}$)[a] [%]	PCE (PCE$_{avg}$)[a] [%]
PBDT-BZ	BDTB-Ph	0.921 (0.918 ± 0.003)	17.62 (17.52 ± 0.12)	17.41	65.2 (64.5 ± 0.6)	10.59 (10.38 ± 0.20)
	BDTB-Na	0.892 (0.888 ± 0.004)	17.85 (17.66 ± 0.21)	17.71	63.6 (62.6 ± 0.5)	10.14 (10.01 ± 0.12)
	TBDB-Ph	0.926 (0.921 ± 0.005)	9.93 (9.81 ± 0.20)	9.74	43.9 (42.8 ± 0.7)	4.04 (3.88 ± 0.14)
	TBDB-Na	0.905 (0.903 ± 0.002)	13.14 (13.02 ± 0.16)	12.98	53.2 (51.6 ± 1.2)	6.32 (6.10 ± 0.18)
PTBD-BZ	BDTB-Ph	0.928 (0.926 ± 0.003)	16.74 (16.54 ± 0.15)	16.43	59.6 (58.5 ± 0.7)	9.26 (9.04 ± 0.20)
	BDTB-Na	0.877 (0.875 ± 0.002)	18.39 (18.25 ± 0.16)	18.03	62.2 (61.0 ± 0.6)	10.03 (9.85 ± 0.16)
	TBDB-Ph	0.925 (0.923 ± 0.002)	18.13 (17.94 ± 0.22)	17.50	65.9 (65.0 ± 0.8)	11.06 (10.92 ± 0.11)
	TBDB-Na	0.906 (0.905 ± 0.002)	19.61 (19.50 ± 0.14)	19.06	70.2 (69.2 ± 0.8)	12.47 (12.25 ± 0.16)
PDTBDT-BZ	BDTB-Ph	0.884 (0.883 ± 0.003)	13.29 (13.20 ± 0.12)	13.16	55.3 (53.9 ± 0.6)	6.50 (6.19 ± 0.25)
	BDTB-Na	0.864 (0.863 ± 0.002)	12.86 (12.72 ± 0.18)	12.84	44.5 (43.2 ± 0.8)	4.95 (4.70 ± 0.20)
	TBDB-Ph	0.913 (0.911 ± 0.003)	13.41 (13.18 ± 0.26)	13.20	51.8 (50.5 ± 1.0)	6.20 (5.97 ± 0.16)
	TBDB-Na	0.879 (0.878 ± 0.002)	11.24 (11.08 ± 0.18)	10.93	54.4 (52.8 ± 1.2)	5.38 (5.13 ± 0.18)

[a]The values in parentheses are the average values with standard deviations obtained from 15 devices. [b]Integrated from the EQE spectrum.

π−π stacking diffraction signal along the in-plane (IP) direction and a strong lamellar packing signal along the OOP direction are observed in the pattern of the PDTBDT-BZ film, signifying its partial edge-on orientation, which may have a negative influence on charge transport and PV performance. PTBD-BZ shows (010) peaks at q_z = 1.80 Å^{-1}, corresponding to a π−π stacking distance of 3.60 Å, which is much smaller than those of PBDT-BZ (3.68 Å) and PDTBDT-BZ (3.71 Å). This result suggests that backbone conformation can strongly change the interchain distance of polymers. These GIWAXS measurements are in good agreement with the theoretical calculation results. Hence, the molecular planarity of the polymers can be tuned by a subtle strategy based on an asymmetric backbone, which can greatly improve the polymer's crystallinity and intermolecular packing. Furthermore, the novel TBD backbone is a promising and competitive structure for application in the photoelectric field.

The molecular geometries of the four acceptors were also optimized by DFT calculation and showed different backbone conformations in the side view and top view. Clearly, the asymmetric small molecules TBDB-Ph and TBDB-Na featured four stretched hexylphenyl substituents on the same side. Because of the asymmetric skeleton, the two twist angles between the TBD core and terminal group are different. When the terminal phenyl (Ph) group was replaced by a naphthalene (Na) group, the conjugation length increased, and the twist angle between the core and terminal group became larger. From the GIWAXS patterns, it can be easily found that the SMAs with TBD as the core show weaker crystallinity than that of the SMAs with the BDT core and that a small conjugated structure was more favorable to form ordered packing than a large conjugated structure (Figure 3). These SMAs with different conformations can facilitate our study on the compatibility of donor and acceptor pairs.

The PV performance of donor−acceptor (D−A) pairs used as the active layer was evaluated by fabricating PSCs with a device structure of ITO (indium-tinoxide)/poly(3,4-ethylenedioxythiophene):poly(styrenesulfonate) (PEDOT:PSS)/active layer/perylenediimide functionalized with amino *N*-oxide (PDINO)/Al. We used CB as the only solvent because it well dissolves all the polymer donors and acceptors. The device processing conditions, including the (D−A) weight ratio and post-treatment, such as thermal annealing or solvent vapor annealing, were carefully investigated, and the detailed

DOI: 10.1021/acsami.9b14981
ACS Appl. Mater. Interfaces 2019, 11, 44501−44512

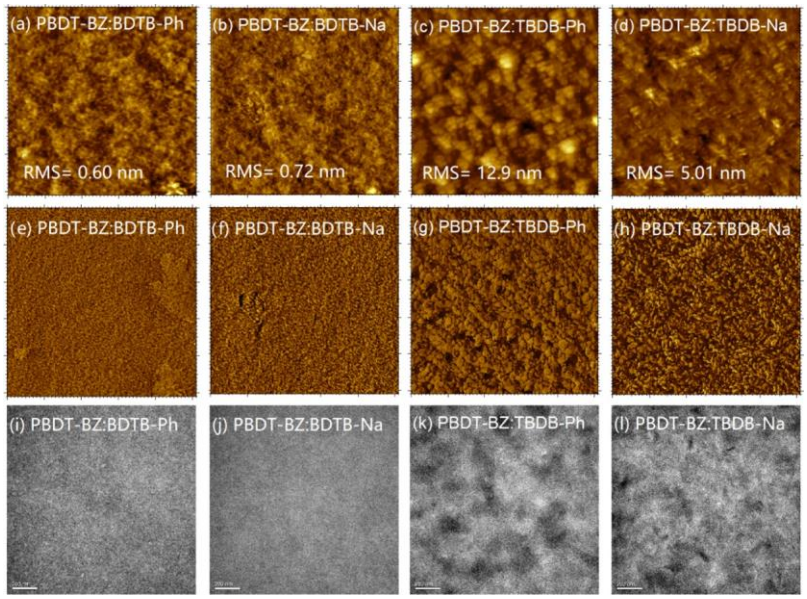

Figure 5. (a−d) Tapping-mode AFM height and (e−h) phase images (5 × 5 μm) of PBDT-BZ-based blend films. (i−l) TEM images of PBDT-BZ-based blend films.

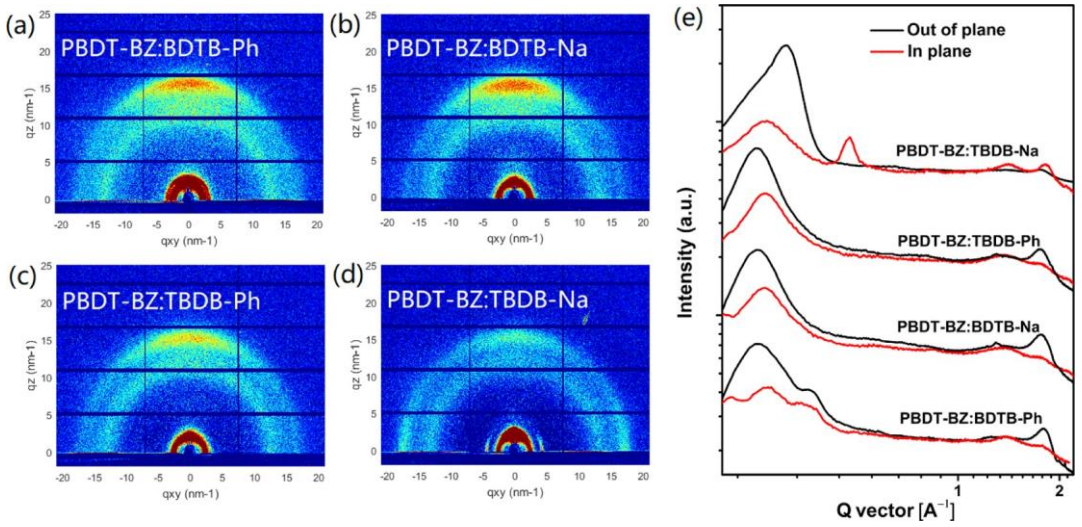

Figure 6. 2D GIWAXS patterns of (a) PBDT-BZ/BDTB-Ph, (b) PBDT-BZ/BDTB-Na, (c) PBDT-BZ/TBDB-Ph, and (d) PBDT-BZ/TBDB-Na blend films. (e) GIWAXS intensity profiles of different PBDT-BZ/SMA blend films along the IP (black lines) and OOP (red lines) directions.

processes are given in SI. The optimal D−A weight ratios are found to be 1:1, 1:1, and 1:1.25 for the PBDT-BZ, PTBD-BZ, and PDTBDT-BZ polymers, respectively. The current density−voltage ($J-V$) and external quantum efficiency (EQE) curves of the PSCs with different D−A pairs are shown in Figure 4, and the detailed PV parameters are collected in Table 2. The corresponding optimized data can be found in Tables S1−S3. The current densities calculated from the EQE measurements agreed well with the J_{sc} values obtained from the $J-V$ measurements. We noted that the PSCs based on PDTBDT-BZ with a zigzag conformation exhibit low PCEs when blended with all four different SMAs. This result reflects that amorphous polymers cannot match well with medium- or low-crystallinity small molecules to form ideal D−A pairs. However, for the medium-crystallinity polymer PBDT-BZ, the performance results were notably distinct in regard to J_{sc} and FF when blended with SMAs having shorter or longer conjugated lengths in their central cores. PBDT-BZ provided decent PCEs over 10% when paired with either BDTB-Ph or BDTB-Na. However, after PBDT-BZ was blended with the asymmetric low-crystallinity SMAs TBDB-Ph and TBDB-Na, the resulting devices presented low PV performance (very low PCEs of 4.04 and 6.32%, respectively) comparable to that of PDTBDT-BZ. In contrast, the highly crystalline polymer PTBD-BZ is well compatible with all the four SMAs, with the PTBD-BZ/TBDB-Na-based device even exhibiting a remarkable PCE of 12.47%. To further study the charge dissociation and collection properties of different D−A pairs, we measured the photocurrent density (J_{ph}) versus the effective voltage (V_{eff}) of the devices (see Figure S4a−c, Supporting Information).[74] It was observed that PDTBDT-BZ-based devices have a competitive saturated photocurrent but poor charge dissociation probability (P_{diss}) in the PV process, implying severe charge recombination and inefficient charge extraction.[75] Conversely, the high P_{diss} values obtained from all PTBD-BZ-based devices reveal favorable charge transport,

DOI: 10.1021/acsami.9b14981
ACS Appl. Mater. Interfaces 2019, 11, 44501−44512

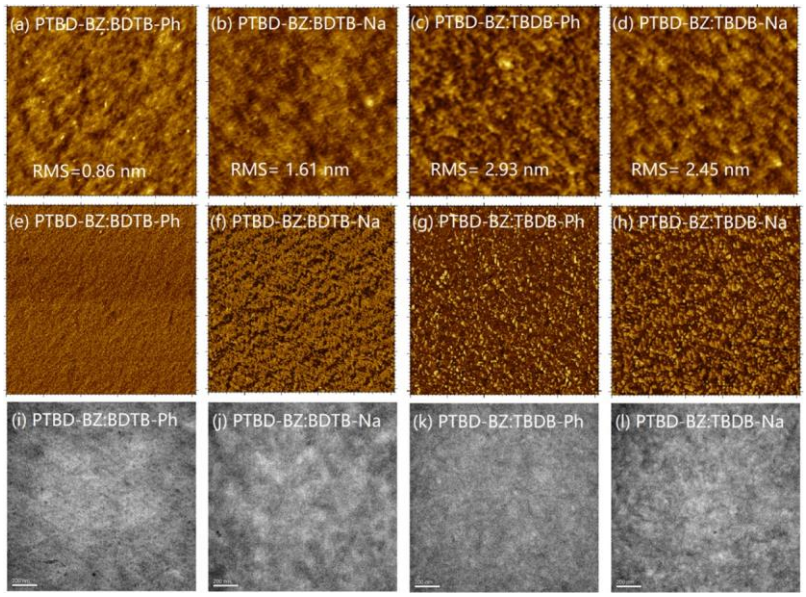

Figure 7. (a−d) Tapping-mode AFM height and (e−h) phase images (5 × 5 μm) of PBDT-BZ-based blend films. (i−l) TEM images of PTBD-BZ-based blend films.

which can be attributed to a balance between the conjugation length (in comparison with PBDT-BZ) and linear conformation (referring to PDTBDT-BZ), thereby resulting in dense packing. Moreover, charge carrier mobility was measured using the space-charge limited current (SCLC) method (see Figures S2 and S3, Supporting Information). The SCLC results (seen in Table S4) provide more direct evidence for the correlation between charge transport and the cooperation of the conjugation length and molecular conformation. The higher mobility of the PTBD-BZ-blended films signifies reduced space charge accumulation and recombination, leading to increased J_{sc} and FF.[76] These results illustrate the critical role of D−A compatibility and inspire us to further study the effect of different D−A conformations on PV performance. Thus, we focus on and discuss the morphology of PBDT-BZ- and PTBD-BZ-based films blended with the four small molecules in the following.

First, the four PBDT-BZ-based blend films were characterized by atomic force microscopy (AFM), transmission electron microscopy (TEM), and GIWAXS analyses. The PBDT-BZ/BDTB-Ph and PBDT-BZ/BDTB-Na films show a smooth surface with an average root-mean-square (rms) roughness of 0.60 and 0.72 nm, while the PBDT-BZ/TBDB-Ph and PBDT-BZ/TBDB-Na films show strongly increased rms roughnesses of 12.9 and 5.01 nm, respectively. The rough surface indicates the disordered microstructure of the blend films. From the phase images (Figure 5e−h) and TEM measurements (Figure 5i−l), we found that the PBDT-BZ/TBDB-Ph and PBDT-BZ/TBDB-Na films display large domains and inhomogeneous phase separation, which signify poor miscibility. This property would increase charge recombination, leading to inferior J_{sc} and FF values. Figure 6a−d depicts 2D GIWAXS patterns of the PBDT-BZ-based BHJ films prepared with the four SMAs. Their scattering profiles are shown in Figure 6e. Although BDTB-Ph and BDTB-Na by themselves show different stacking properties, the diffraction features of their BHJ films blended with PBDT-BZ are quite similar. Notably, the pronounced (010) diffraction peak at q_z = 1.77 Å^{-1} in the OOP direction and broad (100) diffraction peak at approximately q_{xy} = 0.3 Å^{-1} reveal a preferential face-on orientation for both the PBDT-BZ/BDTB-Ph and PBDT-BZ/BDTB-Na blends, which is beneficial for charge transport in the vertical direction. Therefore, the symmetric BDT core can largely retain the molecular orientation of the neat PBDT-BZ films. In contrast, the PBDT-BZ/TBDB-Ph and PBDT-BZ/TBDB-Na films did not reveal high-order π−π stacking peaks, and the peak intensity was quite low. When mixed with SMAs based on the TBD core, the face-on orientation of the neat PBDT-BZ polymer with a moderate intensity (010) peak changes to a mixed face-on and edge-on orientation in the PBDT-BZ/TBDB-Ph and PBDT-BZ/TBDB-Na films, which means that the SMAs based on the asymmetric TBD core strongly influence the stacking and miscibility of PTBD-BZ blend films. In addition, the coherence lengths (CCLs) of the polymer in the PBDT-BZ/BDTB-Ph and PBDT-BZ/BDTB-Na blend films are 3.8 and 3.6 nm, obviously larger than those of the polymer in the PBDT-BZ/TBDB-Ph (2.5 nm) and PBDT-BZ/TBDB-Na (2.0 nm) blend films. These morphology measurements are in accordance with the trend in PBDT-BZ-based device performance.

Subsequently, we examined the morphology of the PTBD-BZ-based blend films. From the AFM images, we can see that all the PTBD-BZ-based blend films have relatively similar aggregated and homogeneous nanostructures. The uniform and moderate domain clusters observed in phase images indicate high compatibilities between PTBD-BZ and each of the four small molecules. Compared with the PTBD-BZ/BDTB-Ph and PTBD-BZ/BDTB-Na blends, the PTBD-BZ/TBDB-Ph and PTBD-BZ/TBDB-Na blends show slightly increased roughness values of 2.93 and 2.54 nm, which may be attributed to the increased pure domain size and slightly reduced miscibility. In the TEM images (Figure 7i−l), the four blend films exhibit the desired nanoscale phase separation and bicontinuous penetrated networks. Obviously, compared with the PBDT-BZ/BDTB-Ph and PBDT-BZ/BDTB-Ph films, the films based on PTBD-BZ and the same small molecules showed more balanced domain size and phase separation,

DOI: 10.1021/acsami.9b14981
ACS Appl. Mater. Interfaces 2019, 11, 44501−44512

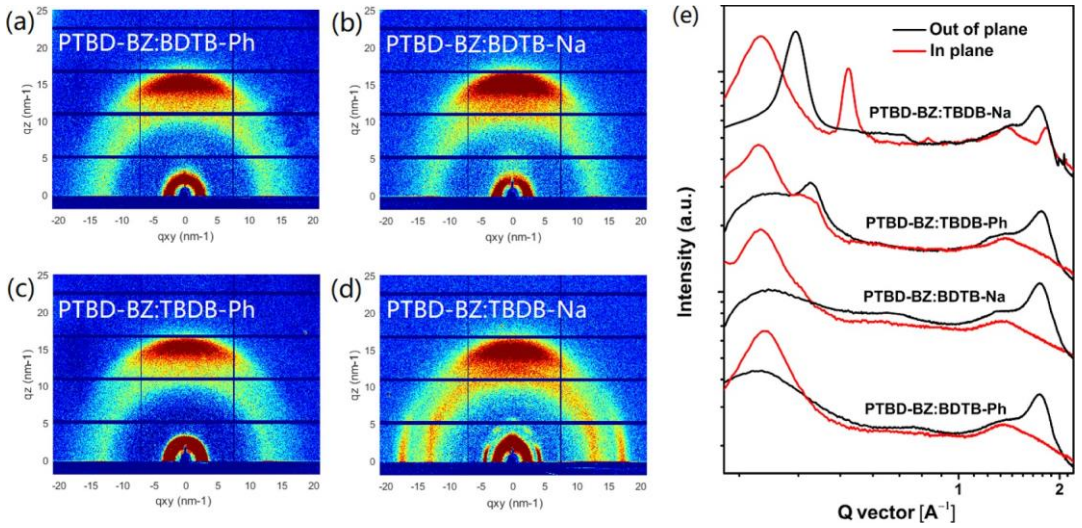

Figure 8. 2D GIWAXS patterns of (a) PTBD-BZ/BDTB-Ph, (b) PTBD-BZ/BDTB-Na, (c) PTBD-BZ/TBDB-Ph, and (d) PTBD-BZ/TBDB-Na blend films. (e) GIWAXS intensity profiles of different PTBD-BZ/SMA blend films along the IP (black lines) and OOP (red lines) directions.

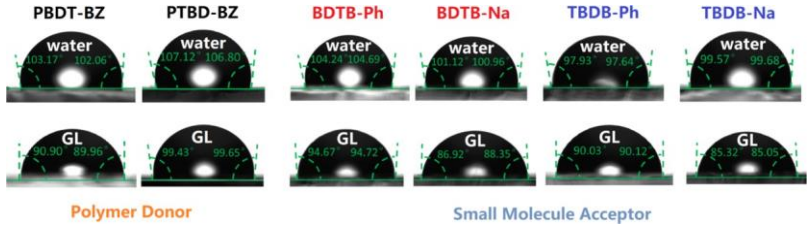

Figure 9. Contact angle measurements for different polymers and SMA neat films.

resulting in remarkable device PCEs of 11.06 and 12.47%, respectively. In addition, a strange and dramatic phenomenon was noted in the GIWAXS pattern (Figure 8): For the four different PBDT-BZ/small molecule blend films, PTBD-BZ can maintain its high crystallinity and even show stronger (010) π−π stacking and (100) lamellar packing than those of the neat film. The CCLs of PTBD-BZ in the BDTB-Ph, BDTB-Na, TBDB-Ph, and TBDB-Na blend films are 7.0, 7.7, 7.3, and 8.1 nm, respectively, which are larger than those of the polymer in the corresponding PBDT-BZ/small molecule blend films. The similar CCLs of PTBD-BZ in different blend films and similar stacking trends reveal that the high-crystallinity polymer PTBD-BZ can match well not only with medium-crystallinity small molecules but also with low-crystallinity and amorphous small molecules. In addition, the strong (100) IP scatting peak of the PTBD-BZ/TBDB-Na blend film at ca. 4.6 nm^{-1} reflects the lamellar stacking of the small molecule TBDB-Na. When the small molecule core was changed from BDT to TBD, the PTBD-BZ/TBDB-Na blend film displays excellent morphology with balanced crystallinity and phase separation despite the poor aggregation of neat TBDB-Na. The GIWAXS results are consistent with the AFM and TEM measurements, providing a convincing explanation for the difference in performance between films based on different D/A pairs.

To further investigate and verify how the conformations of the donor polymer and small molecules influence the miscibility of the blend films, the contact angle and related surface tensions of the films were investigated (Figure 9 and Table 3). The results indicate that the medium-crystallinity PBDT-BZ film has higher surface tension than that of the high-crystallinity PTBD-BZ film, which is confirmed by water and

Table 3. Contact Angle of Water and Glycerol and Surface Tension of Corresponding Polymers and Small Molecules

films	θ [deg]	θ [deg]	γ [mN m^{-1}]	γ [mN m^{-1}]
PBDT-BZ	102.6	90.4	21.48	23.42
PTBD-BZ	106.9	106.9	18.87	18.63
BDTB-Ph	104.4	90.5	20.34	23.12
BDTB-Na	101.0	87.6	22.40	24.90
TBDB-Ph	97.7	90.1	24.32	23.57
TBDB-Na	99.5	85.1	23.04	26.35

glycerol contact angle measurements. The difference in surface tension between the two polymers could be attributed to the different polarities of their backbone conformations. The same trend was also observed among the four small molecules. Previous reports have verified that large differences in surface energy between two phases corresponded to a stronger repulsive interaction, implying relatively poor miscibility. The potential for higher domain purity of the two phases can be quantified by the equation $\chi = (\sqrt{\gamma_{donor}} - \sqrt{\gamma_{acceptor}})^2$, where χ is the Flory−Huggins interaction parameter of the two phases.[77,78] This equation is used to further investigate the miscibility of the blend of the films. When the two polymers PBDT-BZ and PTBD-BZ are mixed with the four small molecules, all the PTBD-BZ-based blends give a much higher χ value than that of the PBDT-BZ-based blends (Table S5), indicating that the PTBD-BZ-based blends possess much higher domain purity but relatively lower miscibility, which strongly agrees with the GIWAXS measurements. In addition, the PTBD-BZ/TBDB-Na-based device providing the best performance may be ascribed to the suitable miscibility

DOI: 10.1021/acsami.9b14981
ACS Appl. Mater. Interfaces 2019, 11, 44501−44512

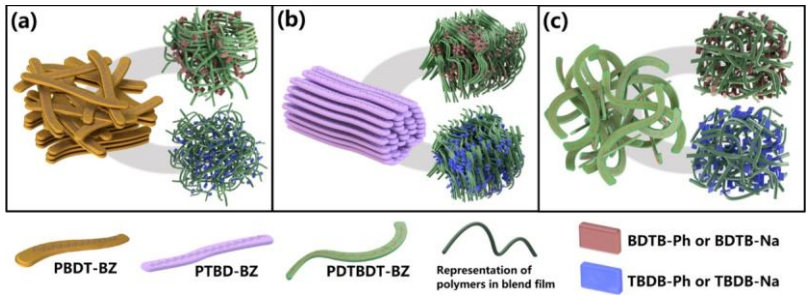

Figure 10. Schematic diagram of the neat polymer and corresponding active layer microstructures. (a) Neat PBDT-BZ film and PBDT-BZ-based blend films. (b) Neat PTBD-BZ film and PTBD-BZ-based blend films. (c) Neat PDTBDT-BZ film and PDTBDT-BZ-based blend films.

between the two components, which can be confirmed by the χ value. Therefore, we can conclude that PTBD-BZ may have advantages over PTBD-BZ in forming pure domains and balancing the miscibility of blend films.

Finally, based on the detailed DFT and morphological analyses, we performed a comparative schematic diagram to clearly demonstrate the compatibility between the donor and acceptor, as shown in Figure 10. The zigzag polymer PDTBDT-BZ with a large angle of 46.4° in the backbone exhibits low crystallinity and weak $\pi-\pi$ stacking and is thus incompatible with all the four small molecules (Figure 10c). The corresponding amorphous blended films lead to reduced charge transport and poor PV performance. The polymer PBDT-BZ with a backbone angle of 32.7° shows moderate crystallinity (Figure 10a). When blended with the two SMAs based on the BDT core, the polymer PBDT-BZ still retains its ordered microstructure and provides decent device performance. However, when blended with the two low-crystallinity small molecules based on the TBD core, PBDT-BZ exhibits complete loss of its original packing properties and converts into a mixed face-on/edge-on orientation in the resulting BHJ films; this chaotic microstructure could result in poor device performance. In contrast, the polymer PTBD-BZ with four asymmetric fused-ring TBD units has extremely small dihedral angles in the backbone and thus displays much stronger and denser intermolecular stacking than the other two polymers. When mixed with symmetric small molecules based on the BDT core or with very low-crystallinity asymmetric small molecules based on the TBD core, higher crystallinity and face-on orientation are afforded, and the pure domain size and miscibility are balanced in the blends (Figure 10b). As a result, high PV performances were achieved by all the PTBD-BZ-based devices. Thus, we can conclude that PTBD-BZ has more extensive compatibility than PBDT-BZ, as the former polymer can match well not only with medium-crystallinity small molecules but also with very low-crystallinity small molecules, demonstrating its remarkable superiority. Conversely, PDTBDT-BZ-based devices perform worse with the majority of the SMAs.

CONCLUSIONS

Three model polymers, PBDT-BZ, PTBD-BZ, and PDTBDT-BZ, were first used to systematically investigate the correlation among polymers' molecular conformation, morphology, and PV properties. Then, four symmetric SMAs based on the BDT core and asymmetric SMAs based on the TBD core were designed to further understand the compatibility of D−A combinations. The GIWAXS measurements indicated that higher crystallinity, more ordered and denser $\pi-\pi$ stacking can be found in the films based on PTBD-BZ than those based on PBDT-BZ and PDTBDT-BZ, which was a result of the more linear backbone conformation of PTBD-BZ. The high morphological order and balance between domain purity and miscibility were evidenced by the good performance of devices based on PTBD-BZ blended with four different small molecules. In particular, the PTBD-BZ/TBDB-Na-based device yielded a high PCE of 12.47%, even though the SMA TBDB-Na had very low crystallinity. On the other hand, the moderately ordered polymer PBDT-BZ was found to have poor compatibility with low-crystallinity small molecules based on the TBD core yet served as a better-performing active layer when blended with small molecules based on the BDT core. Furthermore, because of the large angles in the backbone, all the amorphous donor polymer PDTBDB-BZ-based devices underperformed when combined with various SMAs. Overall, our results clearly delineated the correlation between the morphology of conjugated polymers and their molecular conformations and the structure−property relationship between different donors and acceptors.

EXPERIMENTAL SECTION

Materials. All the reagents, unless otherwise specified, were purchased from Sigma-Aldrich Co., J&K, and Tokyo Chemical Industry Co., Ltd., and were used without further purification. The synthesis details of the small molecule acceptors BDTB-Ph, BDTB-Na, TBDB-Ph and TBDB-Na were collected in the Supporting Information.

ASSOCIATED CONTENT

Supporting Information

The Supporting Information is available free of charge on the ACS Publications website at DOI: 10.1021/acsami.9b14981.

Experimental details for synthesis of materials, material characterization, device fabrication and characterization, and mobility measurement (PDF)

AUTHOR INFORMATION

Corresponding Authors

*E-mail: baoxc@qibebt.ac.cn (X.B.).
*E-mail: yangrq@qibebt.ac.cn (R.Y.).

ORCID

Yonghai Li: 0000-0002-5748-0258
Chunming Yang: 0000-0001-8008-3675
Xichang Bao: 0000-0001-7325-7550
Renqiang Yang: 0000-0001-6794-7416

Notes

The authors declare no competing financial interest.

DOI: 10.1021/acsami.9b14981
ACS Appl. Mater. Interfaces 2019, 11, 44501−44512

ACKNOWLEDGMENTS

The authors are deeply grateful to the National Natural Science Foundation of China (51773220 and 51573205), the Shandong Provincial Natural Science Foundation (ZR2017ZB0314), the Youth Innovation Promotion Association CAS (2016194), DICP & QIBEBT (UN201709 and UN201805), and Dalian National Laboratory for Clean Energy (DNL) CAS for financial support. The authors thank beamline BL16B1 (Shanghai Synchrotron Radiation Facility) for providing beam time. D.Y. thanks the Sino-Danish Center for Education and Research for the support.

REFERENCES

(1) Yan, C.; Barlow, S.; Wang, Z.; Yan, H.; Jen, A. K. Y.; Marder, S. R.; Zhan, X. Non-Fullerene Acceptors for Organic Solar Cells. *Nat. Rev. Mater.* 2018, *3*, 18003.

(2) Lu, L.; Zheng, T.; Wu, Q.; Schneider, A. M.; Zhao, D.; Yu, L. Recent Advances in Bulk Heterojunction Polymer Solar Cells. *Chem. Rev.* 2015, *115*, 12666−12731.

(3) Nielsen, C. B.; Holliday, S.; Chen, H.-Y.; Cryer, S. J.; McCulloch, I. Non-Fullerene Electron Acceptors for Use in Organic Solar Cells. *Acc. Chem. Res.* 2015, *48*, 2803−2812.

(4) Lin, Y.; Zhan, X. Oligomer Molecules for Efficient Organic Photovoltaics. *Acc. Chem. Res.* 2016, *49*, 175−183.

(5) Cheng, P.; Li, G.; Zhan, X.; Yang, Y. Next-Generation Organic Photovoltaics Based on Non-Fullerene Acceptors. *Nat. Photonics* 2018, *12*, 131−142.

(6) Cui, C.; Li, Y. High-Performance Conjugated Polymer Donor Materials for Polymer Solar Cells with narrow-bandgap nonfullerene acceptors. *Energy Environ. Sci.* 2019, *12*, 3225−3246.

(7) Fu, H.; Wang, Z.; Sun, Y. Polymer Donors for High-performance Non-Fullerene Organic Solar Cells. *Angew. Chem., Int. Ed.* 2019, *58*, 4442−4453.

(8) Baran, D.; Ashraf, R. S.; Hanifi, D. A.; Abdelsamie, M.; Gasparini, N.; Röhr, J. A.; Holliday, S.; Wadsworth, A.; Lockett, S.; Neophytou, M.; et al. Reducing the Efficiency-Stability-Cost Gap of Organic Photovoltaics with Highly Efficient and Stable Small Molecule Acceptor Ternary Solar Cells. *Nat. Mater.* 2017, *16*, 363−369.

(9) Meng, L.; Zhang, Y.; Wan, X.; Li, C.; Zhang, X.; Wang, Y.; Ke, X.; Xiao, Z.; Ding, L.; Xia, R.; Yip, H.; Cao, Y.; Cheng, Y. Organic and Solution-Processed Tandem Solar Cells with 17.3% Efficiency. *Science* 2018, *361*, 1094−1098.

(10) Xu, X.; Feng, K.; Bi, Z.; Ma, W.; Zhang, G.; Peng, Q. Single-Junction Polymer Solar Cells with 16.35% Efficiency Enabled by a Platinum(II) Complexation Strategy. *Adv. Mater.* 2019, *31*, 1901872.

(11) Cui, Y.; Yao, H.; Zhang, J.; Zhang, T.; Wang, Y.; Hong, L.; Xian, K.; Xu, B.; Zhang, S.; Peng, J.; Wei, Z.; Gao, F.; Hou, J. Over 16% Efficiency Organic Photovoltaic Cells Enabled by a Chlorinated Acceptor with Increased Open-circuit Voltages. *Nat. Commun.* 2019, *10*, 2515.

(12) Sun, H.; Liu, T.; Yu, J.; Lau, T.-K.; Zhang, G.; Zhang, Y.; Su, M.; Tang, Y.; Ma, R.; Liu, B.; Liang, J.; Feng, K.; Lu, X.; Guo, X.; Gao, F.; Yan, H. A Monothiophene Unit Incorporating Both Fluoro and Ester Substitution Enabling High-performance Donor Polymers for Non-Fullerene Solar Cells with 16.4% Efficiency. *Energy Environ. Sci.* 2019, *12*, 3328−3337.

(13) Yan, T.; Song, W.; Huang, J.; Peng, R.; Huang, L.; Ge, Z. 16.67% Rigid and 14.06% Flexible Organic Solar Cells Enabled by Ternary Heterojunction Strategy. *Adv. Mater.* 2019, *31*, 1902210.

(14) Li, S.; Ye, L.; Zhao, W.; Yan, H.; Yang, B.; Liu, D.; Li, W.; Ade, H.; Hou, J. A Wide Band Gap Polymer with a Deep Highest Occupied Molecular Orbital Level Enables 14.2% Efficiency in Polymer Solar Cells. *J. Am. Chem. Soc.* 2018, *140*, 7159−7167.

(15) Zhang, H.; Yao, H.; Hou, J.; Zhu, J.; Zhang, J.; Li, W.; Yu, R.; Gao, B.; Zhang, S.; Hou, J. Over 14% Efficiency in Organic Solar Cells Enabled by Chlorinated Nonfullerene Small-Molecule Acceptors. *Adv. Mater.* 2018, *30*, 1800613.

(16) Xiao, Z.; Jia, X.; Ding, L. Ternary Organic Solar Cells Offer 14% Power Conversion Efficiency. *Sci. Bull.* 2017, *62*, 1562−1564.

(17) Li, Y.; Zheng, N.; Yu, L.; Wen, S.; Gao, C.; Sun, M.; Yang, R. A Simple Phenyl Group Introduced at the Tail of Alkyl Side Chains of Small Molecular Acceptors: New Strategy to Balance the Crystallinity of Acceptors and Miscibility of Bulk Heterojunction Enabling Highly Efficient Organic Solar Cells. *Adv. Mater.* 2019, *31*, 1807832.

(18) Yuan, J.; Zhang, Y.; Zhou, L.; Zhang, G.; Yip, H.-L.; Lau, T.-K.; Lu, X.; Zhu, C.; Peng, H.; Johnson, P. A.; Leclerc, M.; Cao, Y.; Ulanski, J.; Li, Y.; Zou, Y. Single-Junction Organic Solar Cell with over 15% Efficiency Using Fused-Ring Acceptor with Electron-Deficient Core. *Joule* 2019, *3*, 1140−1151.

(19) Yuan, J.; Zhang, Y.; Zhou, L.; Zhang, C.; Lau, T. K.; Zhang, G.; Lu, X.; Yip, H. L.; So, S. K.; Beaupré, S.; Mainville, M.; Johnson, P. A.; Leclerc, M.; Chen, H.; Peng, H.; Li, Y.; Zou, Y. Fused Benzothiadiazole: A Building Block for n-Type Organic Acceptor to Achieve High-Performance Organic Solar Cells. *Adv. Mater.* 2019, *31*, 1807577.

(20) Lin, Y.; Zhao, F.; Wu, Y.; Chen, K.; Xia, Y.; Li, G.; Prasad, S. K. K.; Zhu, J.; Huo, L.; Bin, H.; Zhang, Z.-G.; Guo, X.; Zhang, M.; Sun, Y.; Gao, F.; Wei, Z.; Ma, W.; Wang, C.; Hodgkiss, J.; Bo, Z.; Inganäs, O.; Li, Y.; Zhan, X. Mapping Polymer Donors toward High-Efficiency Fullerene Free Organic Solar Cells. *Adv. Mater.* 2017, *29*, 1604155.

(21) Kan, B.; Feng, H.; Wan, X.; Liu, F.; Ke, X.; Wang, Y.; Wang, Y.; Zhang, H.; Li, C.; Hou, J.; Chen, Y. Small-Molecule Acceptor Based on the Heptacyclic Benzodi(cyclopentadithiophene) Unit for Highly Efficient Nonfullerene Organic Solar Cells. *J. Am. Chem. Soc.* 2017, *139*, 4929−4934.

(22) Yuan, J.; Huang, T.; Cheng, P.; Zou, Y.; Zhang, H.; Yang, J. L.; Chang, S.; Zhang, Z.; Huang, W.; Wang, R.; Meng, D.; Gao, F.; Yang, Y. Enabling Low Voltage Losses and High Photocurrent in Fullerene-Free Organic Photovoltaics. *Nat. Commun.* 2019, *10*, 1624.

(23) Yao, Z.; Liao, X.; Gao, K.; Lin, F.; Xu, X.; Shi, X.; Zuo, L.; Liu, F.; Chen, Y.; Jen, A. K.-Y. Dithienopicenocarbazole-Based Acceptors for Efficient Organic Solar Cells with Optoelectronic Response Over 1000 nm and an Extremely Low Energy Loss. *J. Am. Chem. Soc.* 2018, *140*, 2054−2057.

(24) Müller, C.; Ferenczi, T. A. M.; Campoy-Quiles, M.; Frost, J. M.; Bradley, D. D. C.; Smith, P.; Stingelin-Stutzmann, N.; Nelson, J. Binary Organic Photovoltaic Blends: A Simple Rationale for Optimum Compositions. *Adv. Mater.* 2008, *20*, 3510−3515.

(25) Wolfer, P.; Schwenn, P. E.; Pandey, A. K.; Fang, Y.; Stingelin, N.; Burn, P. L.; Meredith, P. Identifying the Optimum Composition in Organic Solar Cells Comprising Non-Fullerene Electron Acceptors. *J. Mater. Chem. A* 2013, *1*, 5989−5995.

(26) Huang, Y.; Kramer, E. J.; Heeger, A. J.; Bazan, G. C. Bulk Heterojunction Solar Cells: Morphology and Performance Relationships. *Chem. Rev.* 2014, *114*, 7006−7043.

(27) Kouijzer, S.; Michels, J. J.; van den Berg, M.; Gevaerts, V. S.; Turbiez, M.; Wienk, M. M.; Janssen, R. A. J. Predicting Morphologies of Solution Processed Polymer:Fullerene Blends. *J. Am. Chem. Soc.* 2013, *135*, 12057−12067.

(28) Wang, G.; Swick, S. M.; Matta, M.; Mukherjee, S.; Strzalka, J. W.; Logsdon, J. L.; Fabiano, S.; Huang, W.; Aldrich, T. J.; Yang, T.; Timalsina, A.; Powers-Riggs, N.; Alzola, J. M.; Young, R. M.; Delongchamp, D. M.; Wasielewski, M. R.; Kohlstedt, K. L.; Schatz, G. C.; Melkonyan, F. S.; Facchetti, A.; Marks, T. J. Photovoltaic Blend Microstructure for High Efficiency Post-Fullerene Solar Cells. To Tilt or Not To Tilt? *J. Am. Chem. Soc.* 2019, *141*, 13410−13420.

(29) Lee, J. K.; Ma, W. L.; Brabec, C. J.; Yuen, J.; Moon, J. S.; Kim, J. Y.; Lee, K.; Bazan, G. C.; Heeger, A. J. Processing Additives for Improved Efficiency from Bulk Heterojunction Solar Cells. *J. Am. Chem. Soc.* 2008, *130*, 3619−3623.

(30) Ma, W.; Ye, L.; Zhang, S.; Hou, J.; Ade, H. Competition between Morphological Attributes in the Thermal Annealing and Additive Processing of Polymer Solar Cells. *J. Mater. Chem. C* 2013, *1*, 5023−5030.

DOI: 10.1021/acsami.9b14981
ACS Appl. Mater. Interfaces 2019, 11, 44501−44512

(31) Yu, R.; Yao, H.; Chen, Z.; Xin, J.; Hong, L.; Xu, Y.; Zu, Y.; Ma, W.; Hou, J. Enhanced π−π Interactions of Nonfullerene Acceptors by Volatilizable Solid Additives in Efficient Polymer Solar Cells. *Adv. Mater.* 2019, *31*, 1900477.
(32) Min, J.; Jiao, X.; Ata, I.; Osvet, A.; Ameri, T.; Bäurle, P.; Ade, H.; Brabec, C. J. Time-Dependent Morphology Evolution of Solution-Processed Small Molecule Solar Cells during Solvent Vapor Annealing. *Adv. Energy Mater.* 2016, *6*, 1502579.
(33) Wu, Y.; Li, Z.; Ma, W.; Huang, Y.; Huo, L.; Guo, X.; Zhang, M.; Ade, H.; Hou, J. PDT-S-T: A New Polymer with Optimized Molecular Conformation for Controlled Aggregation and π−π Stacking and Its Application in Efficient Photovoltaic Devices. *Adv. Mater.* 2013, *25*, 3449−3455.
(34) Zhang, S.; Qin, Y.; Uddin, M. A.; Jang, B.; Zhao, W.; Liu, D.; Woo, H. Y.; Hou, J. A Fluorinated Polythiophene Derivative with Stabilized Backbone Conformation for Highly Efficient Fullerene and Non-Fullerene Polymer Solar Cells. *Macromolecules* 2016, *49*, 2993−3000.
(35) Huang, H.; Yang, L.; Facchetti, A.; Marks, T. J. Organic and Polymeric Semiconductors Enhanced by Noncovalent Conformational Locks. *Chem. Rev.* 2017, *117*, 10291−10318.
(36) Wang, X.; Du, Z.; Dou, K.; Jiang, H.; Gao, C.; Han, L.; Yang, R. A Maverick Asymmetrical Backbone with Distinct Flanked Twist Angles Modulating the Molecular Aggregation and Crystallinity for High Performance Nonfullerene Solar Cells. *Adv. Energy Mater.* 2019, *9*, 1802530.
(37) Chen, J.; Wang, L.; Yang, J.; Yang, K.; Uddin, M. A.; Tang, Y.; Zhou, X.; Liao, Q.; Yu, J.; Liu, B.; Woo, H. Y.; Guo, X. Backbone Conformation Tuning of Carboxylate-Functionalized Wide Band Gap Polymers for Efficient Non-Fullerene Organic Solar Cells. *Macromolecules* 2018, *52*, 341−353.
(38) Li, Z.; Jiang, K.; Yang, G.; Lai, J. Y.; Ma, T.; Zhao, J.; Ma, W.; Yan, H. Donor Polymer Design Enables Efficient Non-Fullerene Organic Solar Cells. *Nat. Commun.* 2016, *7*, 13094.
(39) Chen, S.; Liu, Y.; Zhang, L.; Chow, P. C. Y.; Wang, Z.; Zhang, G.; Ma, W.; Yan, H. A Wide-Bandgap Donor Polymer for Highly Efficient Non-Fullerene Organic Solar Cells with a Small Voltage Loss. *J. Am. Chem. Soc.* 2017, *139*, 6298−6301.
(40) Wang, Y.; Liang, Z.; Li, X.; Qin, J.; Ren, M.; Yang, C.; Bao, X.; Xia, Y.; Li, J. Self-Doping n-type Polymer as Cathode Interface Layer Enables Efficient Organic Solar Cells by Increasing Built-in Electric Field and Boosting Interface Contact. *J. Mater. Chem. C* 2019, *7*, 11152−11159.
(41) Zhu, D.; Wang, Q.; Wang, Y.; Bao, X.; Qiu, M.; Shahid, B.; Li, Y.; Yang, R. Thiazole-Induced Quinoid Polymers for Efficient Solar Cells: Influence of Molecular Skeleton, Regioselectivity, and Regioregularity. *Chem. Mater.* 2018, *30*, 4639−4645.
(42) Chen, W.; Huang, G.; Li, X.; Li, Y.; Wang, H.; Jiang, H.; Zhao, Z.; Yu, D.; Wang, E.; Yang, R. Revealing the Position Effect of an Alkylthio Side Chain in Phenyl-Substituted Benzodithiophene-Based Donor Polymers on the Photovoltaic Performance of Non-Fullerene Organic Solar Cells. *ACS Appl. Mater. Interfaces* 2019, *11*, 33173−33178.
(43) Firdaus, Y.; Maffei, L. P.; Cruciani, F.; Müller, M. A.; Liu, S.; Lopatin, S.; Wehbe, N.; Ndjawa, G. O. N.; Amassian, A.; Laquai, F.; Beaujuge, P. M. Polymer Main-Chain Substitution Effects on the Efficiency of Nonfullerene BHJ Solar Cells. *Adv. Energy Mater.* 2017, *7*, 1700834.
(44) Mai, J.; Xiao, Y.; Zhou, G.; Wang, J.; Zhu, J.; Zhao, N.; Zhan, X.; Lu, X. Hidden Structure Ordering Along Backbone of Fused-Ring Electron Acceptors Enhanced by Ternary Bulk Heterojunction. *Adv. Mater.* 2018, *30*, 1802888.
(45) Zhang, Z.; Yu, J.; Yin, X.; Hu, Z.; Jiang, Y.; Sun, J.; Zhou, J.; Zhang, F.; Russell, T. P.; Liu, F.; Tang, W. Conformation Locking on Fused-Ring Electron Acceptor for High-Performance Nonfullerene Organic Solar Cells. *Adv. Funct. Mater.* 2018, *28*, 1705095.
(46) Wang, J.; Wang, W.; Wang, X.; Wu, Y.; Zhang, Q.; Yan, C.; Ma, W.; You, W.; Zhan, X. Enhancing Performance of Nonfullerene Acceptors via Side-Chain Conjugation Strategy. *Adv. Mater.* 2017, *29*, 1702125.
(47) Yao, H.; Ye, L.; Hou, J.; Jang, B.; Han, G.; Cui, Y.; Su, G. M.; Wang, C.; Gao, B.; Yu, R.; Zhang, H.; Yi, Y.; Woo, H. Y.; Ade, H.; Hou, J. Achieving Highly Efficient Nonfullerene Organic Solar Cells with Improved Intermolecular Interaction and Open-Circuit Voltage. *Adv. Mater.* 2017, *29*, 1700254.
(48) Dai, S.; Li, T.; Wang, W.; Xiao, Y.; Lau, T.-K.; Li, Z.; Liu, K.; Lu, X.; Zhan, X. Enhancing the Performance of Polymer Solar Cells via Core Engineering of NIR-Absorbing Electron Acceptors. *Adv. Mater.* 2018, *30*, 1706571.
(49) Feng, H.; Yi, Y.-Q.-Q.; Ke, X.; Zhang, Y.; Wan, X.; Li, C.; Chen, Y. Synergistic Modifications of Side Chains and End Groups in Small Molecular Acceptors for High Efficient Non-Fullerene Organic Solar Cells. *Sol. RRL* 2018, *2*, 1800053.
(50) Wang, J.; Zhang, J.; Xiao, Y.; Xiao, T.; Zhu, R.; Yan, C.; Fu, Y.; Lu, G.; Lu, X.; Marder, S. R.; Zhan, X. Effect of Isomerization on High-Performance Nonfullerene Electron Acceptors. *J. Am. Chem. Soc.* 2018, *140*, 9140−9147.
(51) Li, S.; Ye, L.; Zhao, W.; Liu, X.; Zhu, J.; Ade, H.; Hou, J. Design of a New Small-Molecule Electron Acceptor Enables Efficient Polymer Solar Cells with High Fill Factor. *Adv. Mater.* 2017, *29*, 1704051.
(52) Feng, H.; Qiu, N.; Wang, X.; Wang, Y.; Kan, B.; Wan, X.; Zhang, M.; Xia, A.; Li, C.; Liu, F.; Zhang, H.; Chen, Y. An A-D-A Type Small-Molecule Electron Acceptor with End-Extended Conjugation for High Performance Organic Solar Cells. *Chem. Mater.* 2017, *29*, 7908−7917.
(53) Xie, D.; Liu, T.; Gao, W.; Zhong, C.; Huo, L.; Luo, Z.; Wu, K.; Xiong, W.; Liu, F.; Sun, Y.; Yang, C. A Novel Thiophene-Fused Ending Group Enabling an Excellent Small Molecule Acceptor for High-Performance Fullerene-Free Polymer Solar Cells with 11.8% Efficiency. *Sol. RRL* 2017, *1*, 1700044.
(54) Lin, Y.; Zhao, F.; He, Q.; Huo, L.; Wu, Y.; Parker, T. C.; Ma, W.; Sun, Y.; Wang, C.; Zhu, D.; Heeger, A. J.; Marder, S. R.; Zhan, X. High-Performance Electron Acceptor with Thienyl Side Chains for Organic Photovoltaics. *J. Am. Chem. Soc.* 2016, *138*, 4955−4961.
(55) Lv, R.; Chen, D.; Liao, X.; Chen, L.; Chen, Y. A Terminally Tetrafluorinated Nonfullerene Acceptor for Well-Performing Alloy Ternary Solar Cells. *Adv. Funct. Mater.* 2019, *29*, 1805872.
(56) Geng, R.; Song, X.; Feng, H.; Yu, J.; Zhang, M.; Gasparini, N.; Zhang, Z.; Liu, F.; Baran, D.; Tang, W. Nonfullerene Acceptor for Organic Solar Cells with Chlorination on Dithieno[3,2-b:2′,3′-d]pyrrol Fused-Ring. *ACS Energy Lett.* 2019, *4*, 763−770.
(57) Li, S.; Zhan, L.; Liu, F.; Ren, J.; Shi, M.; Li, C.-Z.; Russell, T. P.; Chen, H. An Unfused-Core-Based Nonfullerene Acceptor Enables High-Efficiency Organic Solar Cells with Excellent Morphological Stability at High Temperatures. *Adv. Mater.* 2018, *30*, 1705208.
(58) Liu, F.; Zhang, J.; Wang, Y.; Chen, S.; Zhou, Z.; Yang, C.; Gao, F.; Zhu, X. Modulating Structure Ordering via Side-Chain Engineering of Thieno[3,4-b]thiophene-Based Electron Acceptors for Efficient Organic Solar Cells with Reduced Energy Losses. *ACS Appl. Mater. Interfaces* 2019, *11*, 35193−35200.
(59) Wang, R.; Yuan, J.; Wang, R.; Han, G.; Huang, T.; Huang, W.; Xue, J.; Wang, H. C.; Zhang, C.; Zhu, C.; Cheng, P.; Meng, D.; Yi, Y.; Wei, K. H.; Zou, Y.; Yang, Y. Rational Tuning of Molecular Interaction and Energy Level Alignment Enables High-Performance Organic Photovoltaics. *Adv. Mater.* 2019, *31*, 1904215.
(60) Lin, Y.; Wang, J.; Zhang, Z.-G.; Bai, H.; Li, Y.; Zhu, D.; Zhan, X. An Electron Acceptor Challenging Fullerenes for Efficient Polymer Solar Cells. *Adv. Mater.* 2015, *27*, 1170−1174.
(61) Aldrich, T. J.; Matta, M.; Zhu, W.; Swick, S. M.; Stern, C. L.; Schatz, G. C.; Facchetti, A.; Melkonyan, F. S.; Marks, T. J. Fluorination Effects on Indacenodithienothiophene Acceptor Packing and Electronic Structure, End-Group Redistribution, and Solar Cell Photovoltaic Response. *J. Am. Chem. Soc.* 2019, *141*, 3274−3287.
(62) Kan, B.; Zhang, J.; Liu, F.; Wan, X.; Li, C.; Ke, X.; Wang, Y.; Feng, H.; Zhang, Y.; Long, G.; Friend, R. H.; Bakulin, A. A.; Chen, Y. Fine-Tuning the Energy Levels of a Nonfullerene Small-Molecule

DOI: 10.1021/acsami.9b14981
ACS Appl. Mater. Interfaces 2019, 11, 44501−44512

Acceptor to Achieve a High Short-Circuit Current and a Power Conversion Efficiency over 12% in Organic Solar Cells. *Adv. Mater.* 2018, *30*, 1704904.
(63) Liao, X.; Yao, Z.; Gao, K.; Shi, X.; Zuo, L.; Zhu, Z.; Chen, L.; Liu, F.; Chen, Y.; Jen, A. K.-Y. Mapping Nonfullerene Acceptors with a Novel Wide Bandgap Polymer for High Performance Polymer Solar Cells. *Adv. Energy Mater.* 2018, *8*, 1801214.
(64) Liu, T.; Gao, W.; Wang, Y.; Yang, T.; Ma, R.; Zhang, G.; Zhong, C.; Ma, W.; Yan, H.; Yang, C. Unconjugated Side-Chain Engineering Enables Small Molecular Acceptors for Highly Efficient Non-Fullerene Organic Solar Cells: Insights into the Fine-Tuning of Acceptor Properties and Micromorphology. *Adv. Funct. Mater.* 2019, *29*, 1902155.
(65) Min, J.; Zhang, Z.-G.; Zhang, S.; Li, Y. Conjugated Side-Chain-Isolated D−A Copolymers Based on Benzo[1,2-b:4,5-b′]dithiophene-alt-dithienylbenzotriazole: Synthesis and Photovoltaic Properties. *Chem. Mater.* 2012, *24*, 3247−3254.
(66) Bin, H.; Zhang, Z.-G.; Gao, L.; Chen, S.; Zhong, L.; Xue, L.; Yang, C.; Li, Y. Non-Fullerene Polymer Solar Cells Based on Alkylthio and Fluorine Substituted 2D-conjugated Polymers Reach 9.5% Efficiency. *J. Am. Chem. Soc.* 2016, *138*, 4657−4664.
(67) Zhang, Z.-G.; Li, Y. Side-Chain Engineering of High-Efficiency Conjugated Polymer Photovoltaic Materials. *Sci. China Chem.* 2015, *58*, 192−209.
(68) Liu, T.; Pan, X.; Meng, X.; Liu, Y.; Wei, D.; Ma, W.; Huo, L.; Sun, X.; Lee, T. H.; Huang, M.; Choi, H.; Kim, J. Y.; Choy, W. C.; Sun, Y. Alkyl Side-Chain Engineering in Wide-Bandgap Copolymers Leading to Power Conversion Efficiencies over 10%. *Adv. Mater.* 2017, *29*, 1604251.
(69) Cui, C.; Wong, W.-Y.; Li, Y. Improvement of Open-Circuit Voltage and Photovoltaic Properties of 2D-Conjugated Polymers by Alkylthio Substitution. *Energy Environ. Sci.* 2014, *7*, 2276−2284.
(70) Ye, L.; Zhang, S.; Zhao, W.; Yao, H.; Hou, J. Highly Efficient 2D-Conjugated Benzodithiophene-Based Photovoltaic Polymer with Linear Alkylthio Side Chain. *Chem. Mater.* 2014, *26*, 3603−3605.
(71) Gao, P.; Tong, J.; Guo, P.; Li, J.; Wang, N.; Li, C.; Ma, X.; Zhang, P.; Wang, C.; Xia, Y. Medium Band Gap Conjugated Polymers from Thienoacene Derivatives and Pentacyclic Aromatic Lactam as Promising Alternatives of Poly(3-hexylthiophene) in Photovoltaic Application. *J. Polym. Sci., Part A: Polym. Chem.* 2018, *56*, 85−95.
(72) Zhu, D.; Bao, X.; Zhu, Q.; Gu, C.; Qiu, M.; Wen, S.; Wang, J.; Shahid, B.; Yang, R. Thienothiophene-based Copolymers for High-Performance Solar Cells, Employing Different Orientations of the Thiazole Group as a π Bridge. *Energy Environ. Sci.* 2017, *10*, 614−620.
(73) Fei, Z.; Boufflet, P.; Wood, S.; Wade, J.; Moriarty, J.; Gann, E.; Ratcliff, E. L.; McNeill, C. R.; Sirringhaus, H.; Kim, J.-S.; Heeney, M. Influence of Backbone Fluorination in Regioregular Poly(3-alkyl-4-fluoro)thiophenes. *J. Am. Chem. Soc.* 2015, *137*, 6866−6879.
(74) Wu, J.-L.; Chen, F.-C.; Hsiao, Y.-S.; Chien, F.-C.; Chen, P.; Kuo, C.-H.; Huang, M. H.; Hsu, C.-S. Surface Plasmonic Effects of Metallic Nanoparticles on the Performance of Polymer Bulk Heterojunction Solar Cells. *ACS Nano* 2011, *5*, 959−967.
(75) Sun, J.; Ma, X.; Zhang, Z.; Yu, J.; Zhou, J.; Yin, X.; Yang, L.; Geng, R.; Zhu, R.; Zhang, F.; Tang, W. Dithieno[3,2-b:2′,3′-d]pyrrol Fused Nonfullerene Acceptors Enabling Over 13% Efficiency for Organic Solar Cells. *Adv. Mater.* 2018, *30*, 1707150.
(76) Proctor, C. M.; Love, J. A.; Nguyen, T.-Q. Mobility Guidelines for High Fill Factor Solution-Processed Small Molecule Solar Cells. *Adv. Mater.* 2014, *26*, 5957−5961.
(77) Nilsson, S.; Bernasik, A.; Budkowski, A.; Moons, E. Morphology and Phase Segregation of Spin-Casted Films of Polyfluorene/PCBM Blends. *Macromolecules* 2007, *40*, 8291−8301.
(78) Ye, L.; Hu, H.; Ghasemi, M.; Wang, T.; Collins, B. A.; Kim, J.-H.; Jiang, K.; Carpenter, J. H.; Li, H.; Li, Z.; McAfee, T.; Zhao, J.; Chen, X.; Lai, J. L. Y.; Ma, T.; Bredas, J.-L.; Yan, H.; Ade, H. Quantitative Relations Between Interaction Parameter, Miscibility and Function in Organic Solar Cells. *Nat. Mater.* 2018, *17*, 253−260.

DOI: 10.1021/acsami.9b14981
ACS Appl. Mater. Interfaces 2019, 11, 44501−44512